Near-Infrared Spectroscopy of Very Low-Luminosity Young Stellar Objects in the Taurus Molecular Cloud

Itoh, Yoichi

Tamura, Motohide

Alan T. Tokunaga

PASJ: Publ. Astron. Soc. Japan **54**, 561–574, 2002 August 25

Near-Infrared Spectroscopy of Very Low-Luminosity Young Stellar Objects in the Taurus Molecular Cloud

Yoichi ITOH
Graduate School of Science and Technology, Kobe University, 1-1 Rokkodai, Nada, Kobe, Hyogo 657-8501
yitoh@kobe-u.ac.jp
Motohide TAMURA
National Astronomical Observatory, 2-21-1 Osawa, Mitaka, Tokyo 181-8588
tamuramt@cc.nao.ac.jp
and
Alan T. TOKUNAGA
Institute for Astronomy, University of Hawaii, 2680 Woodlawn Drive, Honolulu, Hawaii 96822, USA
tokunaga@ifa.hawaii.edu

(Received 2002 February 4; accepted 2002 May 11)

Abstract

We carried out near-infrared spectroscopic observations of 23 very low-luminosity young stellar object (YSO) candidates and 5 of their companions in Heiles Cloud 2, one of the densest parts of the Taurus molecular cloud. Twelve objects were confirmed to be YSOs by the Bγ feature. The effective temperatures of the YSOs and of the companions are estimated from the 2.26-μm feature, the 2.21-μm feature, and the H_2O band strengths. Detailed comparisons of our photometric and spectroscopic observations with evolutionary tracks on the HR diagram suggest some objects to be very low-mass YSOs.

Key words: infrared: stars — stars: formation — stars: low-mass, brown dwarfs

1. Introduction

Recent optical and near-infrared photometric studies have revealed faint populations of young stellar object (YSO) candidates in low-mass star-forming regions (Comeron et al. 1993; Strom et al. 1995; Itoh et al. 1996, hereafter ITG; Barsony et al. 1997; Oasa et al. 1999), in intermediate-mass star-forming regions (Aspin et al. 1994), and even in high-mass star-forming regions (Kaifu et al. 2000; Lucas, Roche 2000; Oasa 2001). Their faintness is suggestive of low-mass; they may be very low-mass young stars near the stellar/substellar boundary, young brown dwarfs, or even free floating planets.

From photometric observations alone, however, it is impossible to simultaneously determine the mass and age of a YSO. Near-infrared spectroscopy of YSO candidates is necessary to overcome this difficulty (Greene, Meyer 1995; Luhman et al. 1997; Luhman, Rieke 1998; Luhman et al. 1998; Wilking et al. 1999; Cushing et al. 2000; Lucas et al. 2001). The spectra of some faint YSO candidates exhibit absorption features distinctive to the late spectral types, implying young brown dwarfs. While such very low-mass objects may be ubiquitous in star-forming regions, details of the formation process of such objects, for example the mass function, object density, and disk property, are still unknown.

Briceño et al. (1998) have carried out an optical search for very low-mass YSOs in the L 1495, L 1529, L 1551, and B 209 regions in the Taurus molecular cloud. From photometry with spectroscopy, they found 9 new YSOs in the clouds, half of which have very late spectral types, implying very low-mass objects (0.05 $M_\odot$–0.25 $M_\odot$). Luhman (2000) further investigated very low-mass YSOs in the same clouds by combining optical imaging with near-infrared spectroscopy. They found that the mass function of the YSOs in these regions has a peak at 0.8 $M_\odot$, and is relatively flat between the 0.1 $M_\odot$ and 0.8 $M_\odot$ range. In these papers, however, because the targets for the spectroscopy were fully or partially selected based on the optical color–magnitude diagram, the sample may not be complete, especially for embedded very low-mass objects.

ITG conducted a near-infrared survey of the central $1^\circ \times 1^\circ$ region of Heiles Cloud 2 in the Taurus molecular cloud, one of the best-studied low-mass star-forming regions, with a limiting magnitude of 13.4 mag in the K-band. Fifty YSO candidates were identified by their intrinsic red color on the ($J-H$, $H-K$) color–color diagram, following a scheme discussed by Strom et al. (1993). Successive high-resolution imaging surveys discovered 5 companion candidates around the YSO candidates (Itoh et al. 1999). The faintness of some YSOs and their companions may be indicative of the low-mass of the objects.

We describe here a near-infrared spectroscopic follow-up of these faint YSO candidates in Heiles Cloud 2. The observations are described in section 2, and data reduction procedures in section 3. In section 4, we derive effective temperatures of the YSOs, mainly from the 2.21-μm feature, the 2.26-μm feature, and the H_2O absorption band. We also calculate photospheric luminosity of the YSOs from the previous photometry, then plot the YSOs on an HR diagram.

2. Observations

2.1. UKIRT Observations

Twenty-one YSO candidates were selected for spectroscopic observations (table 1). The sample is nearly flux-limited. The

Table 1. YSO sample in Heiles Cloud 2.

ITG No.	α (1950)	δ (1950)	K	$J-H$	$H-K$	A_V	Obs.*	Remark†
2	$4^h34^m57\overset{s}{.}0$	$25^\circ53'01''$	10.05 ± 0.01	0.84 ± 0.01	0.60 ± 0.01	0.14 ± 0.49	U	
4	4 35 15.0	26 01 28	11.05 ± 0.02	2.07 ± 0.05	1.29 ± 0.03	11.42 ± 0.55	U	
5	4 35 17.1	25 46 06	8.31 ± 0.00	1.17 ± 0.01	0.72 ± 0.01	3.38 ± 0.47	U	Kim 1-19
6	4 35 17.5	26 03 19	10.37 ± 0.01	0.96 ± 0.02	0.87 ± 0.02	0.14 ± 0.49	U	GM Tau
9A	4 35 56.6	25 27 17	12.53 ± 0.03	0.88 ± 0.04	0.66 ± 0.04	0.27 ± 0.42	S	
9B	4 35 56.6	25 27 21	14.45 ± 0.03	0.70 ± 0.04	0.70 ± 0.04	0.00 ± 0.39	S	separation = $4\overset{''}{.}31$
13	4 36 15.2	25 31 44	11.69 ± 0.02	0.84 ± 0.03	0.55 ± 0.03	0.36 ± 0.51	U	
15A	4 36 40.5	25 56 02	9.02 ± 0.00	0.86 ± 0.01	0.62 ± 0.01	0.19 ± 0.47	U, S	
15B	4 36 40.4	25 56 06	14.50 ± 0.01	1.01 ± 0.02	0.73 ± 0.02	1.48 ± 0.39	S	separation = $2\overset{''}{.}99$
17	4 36 43.1	25 55 49	10.37 ± 0.01	0.96 ± 0.02	0.82 ± 0.02	0.45 ± 0.49	U	
18	4 36 46.3	25 41 02	10.27 ± 0.01	1.96 ± 0.03	1.18 ± 0.02	10.6 ± 0.50	U	
21	4 36 57.5	25 50 38	10.83 ± 0.01	1.49 ± 0.03	0.94 ± 0.02	6.21 ± 0.51	U	GKH 5
24	4 37 03.6	26 01 26	13.05 ± 0.05	1.01 ± 0.09	0.70 ± 0.09	1.65 ± 0.82	U	
25A	4 37 03.8	25 59 38	8.97 ± 0.00	1.97 ± 0.01	1.37 ± 0.01	9.82 ± 0.49	U,S	IRAS 04370+2559
25B	4 37 03.6	25 59 36	13.38 ± 0.01	2.14 ± 0.01	1.28 ± 0.01	12.29 ± 0.38	S	separation = $4\overset{''}{.}29$
27	4 37 32.7	25 52 34	8.46 ± 0.00	1.04 ± 0.00	0.64 ± 0.00	2.28 ± 0.47	U	
28	4 37 46.2	25 13 16	11.87 ± 0.02	0.81 ± 0.04	0.53 ± 0.04	0.09 ± 0.54	U	
29	4 37 52.5	25 16 19	10.74 ± 0.01	0.86 ± 0.01	0.54 ± 0.01	0.63 ± 0.49	U	
33A	4 38 04.2	25 50 23	11.50 ± 0.02	1.41 ± 0.04	1.19 ± 0.03	3.94 ± 0.55	U, S	
33B	4 38 04.1	25 50 28	16.05 ± 0.02	0.79 ± 0.04	0.54 ± 0.03	0.00 ± 0.41	S	separation = $5\overset{''}{.}17$
36	4 38 10.0	25 12 27	11.01 ± 0.02	0.86 ± 0.02	0.54 ± 0.02	0.63 ± 0.49	U	
39	4 38 16.4	25 28 24	11.80 ± 0.02	1.01 ± 0.03	0.66 ± 0.03	1.88 ± 0.51	U	
40	4 38 20.8	25 38 10	11.47 ± 0.02	2.80 ± 0.18	1.99 ± 0.05	16.68 ± 0.83	U	GKH 32
41	4 38 34.6	25 50 46	9.72 ± 0.01	1.66 ± 0.01	1.11 ± 0.01	7.38 ± 0.49	U	IRAS 04385+2550
43	4 38 39.8	25 27 30	11.24 ± 0.01	0.84 ± 0.01	0.53 ± 0.01	2.97 ± 0.55	U	
45A	4 38 45.3	25 42 37	12.77 ± 0.05	0.90 ± 0.06	0.73 ± 0.07	0.21 ± 0.52	S	
45B	4 38 45.2	25 42 37	15.76 ± 0.05	1.33 ± 0.08	0.91 ± 0.09	4.42 ± 0.62	S	separation = $2\overset{''}{.}29$
46	4 38 52.3	25 47 16	11.01 ± 0.01	0.83 ± 0.01	0.52 ± 0.01	0.41 ± 0.49	U	

* U: UKIRT, S: Subaru.
† GKH: Gomez et al. (1994), Kim: Kim (1990).

K-band magnitudes range from 8 to 12, up to 4 mag fainter than that of classical T Tauri Stars (CTTSs) in the Taurus molecular cloud. We missed ITG 8 and ITG 34, probably due to errors in the coordinates. As template stars, 3 late-type CTTSs, 1 class I source, and 7 late-type dwarfs were also observed.

Spectroscopic observations were carried out during 1996 November 24–26 using the UK Infrared Telescope (UKIRT) at the summit of Mauna Kea, with the Cooled Grating Spectrometer 4 (CGS4, Mountain et al. 1990). CGS4 has a 256×256 InSb array with a spatial scale of $1\overset{''}{.}22\,\mathrm{pixel}^{-1}$. A 75 line mm^{-1} grating was used with a $1\overset{''}{.}2$ slit, providing a wavelength coverage of 1.8 μm–2.5 μm with a resolution R ($=\lambda/\Delta\lambda$) of 300 at 2.21 μm. The integration time used for each source was typically 1–20 seconds, depending on the source brightness. In most cases, 96 exposures were taken for each object. Nodding of the telescope was carried out approximately $16''$ along the slit for sky subtraction. For the YSO candidates and CTTSs, SAO 76542 (A2 V) was observed for a correction of the effects of telluric absorption. For late-type dwarfs, we observed stars with spectral types of A0 V–A3 V at similar airmass. Exposures of an incandescent lamp on and off were taken at the start of each night as dome flats. Exposures of a krypton lamp were taken every three or four hours for wavelength calibrations.

2.2. *Subaru Observations*

The observed objects are 5 binary candidates listed in Itoh et al. (1999) (table 1). The K-band magnitudes of the companions range from 13 to 16. Six late-type dwarfs were also observed as templates, among which 3 latest dwarfs were observed both with UKIRT and Subaru.

Spectroscopic observations were carried out on 2000 December 4–5 with the Infrared Camera and Spectrograph (IRCS, Tokunaga et al. 1998; Kobayashi et al. 2000) on the Subaru Telescope at the summit of Mauna Kea, Hawaii. IRCS has a 1024×1024 InSb array with a spatial scale of $0\overset{''}{.}058\,\mathrm{pixel}^{-1}$. The typical seeing size was $0\overset{''}{.}4$ with a stable condition for both observing dates, so that all binaries were well separated. The grating provided a wavelength coverage of 2.0 μm–2.5 μm. The resolving power, R, was around 350 at 2.2 μm. Because the slit width was $0\overset{''}{.}6$, slightly wider than the seeing size, the effective spectral resolution might change by the seeing size. We measured the FWHMs of the absorption features in each spectrum for each object, and confirmed that the FWHMs do not change in 1 pixel resolution

(~ 6 Å). Therefore, the effective spectral resolution was stable during observations of each target. The integration time used for each source was typically 60–300 seconds, depending on the source brightness. Eight or twelve exposures were taken for each object with the telescope dithered approximately 7.″5 along the slit for sky subtraction. For the binary candidates, SAO 76542 was observed for correcting the effects of telluric absorption. For late-type dwarfs, we observed stars with spectral types of A0 V–A3 V at similar airmass. Exposures of an incandescent lamp on and off were taken at the end of each night as dome flats. Exposures of an argon lamp were taken for wavelength calibrations at the end of each night.

3. Data Reduction and Results

The Image Reduction and Analysis Facility (IRAF) software was used for all data reduction. The reduction procedure was similar for both UKIRT and Subaru data. First, a dithered pair of object frames were subtracted from each other, then divided by flat fields. Next, the data frames were geometrically transformed to correct the curvature of the slit image caused by the grating. The solutions of the geometric transformation and the wavelength calibration were derived from the spectrum of a krypton lamp or argon lamp taken closest in time to the object. Then, individual spectra were extracted from the transformed images using the APALL task. The region where the intensity of the object was more than 20% of the peak intensity at each wavelength was summed into a one-dimensional spectrum. The extracted spectra were then normalized and combined to produce the final spectra. Low signal-to-noise spectra due to the tracking error of the telescope were rejected. The object spectrum was divided by the standard star spectrum, in which the Brackett γ absorption line at 2.166 μm was removed by interpolating across the adjacent continuum with the SPLOT task. Finally, the spectrum was multiplied by a blackbody spectrum of a temperature appropriate to the spectral type of the standard star (Tokunaga 2000).

The K-band spectra of the 23 YSO candidates, 5 companion candidates, 3 CTTSs, a protostar, and 10 late-type dwarfs are shown in figures 1 and 2. Prominent features in the spectra are the Bγ (2.17 μm), 2.21-μm feature, 2.26-μm feature, CO band (2.29 μm and longer), and H_2O absorption ($< 2.15\,\mu$m and $> 2.3\,\mu$m).

Equivalent widths of the Bγ line, the 2.21-μm feature, and the 2.26-μm feature were measured with SPLOT task by Gaussian fitting. On the other hand, equivalent widths of the CO (2–0) band and the CO (4–2) band were calculated by simple integration of the absorption intensity. The uncertainties were estimated from a continuum fit, in which locating the continuum level was the main factor contributing to the equivalent-width uncertainty. We also calculated reddening-independent indices of the H_2O band strength, Q, following Wilking et al. (1999). For Koornneef's extinction law (Koornneef 1983), the Q index is written as

$$Q = \left(\frac{F_1}{F_2}\right)\left(\frac{F_3}{F_2}\right)^{1.24}, \quad (1)$$

where F_1, F_2, and F_3 are the flux densities between 2.07 μm–2.13 μm, 2.267 μm–2.285 μm, and 2.40 μm–2.45 μm.

The measured equivalent widths of the features and the strengths of the bands are tabulated in table 2. The signal-to-noise ratio derived from deviations between each exposure is typically 60 (table 2). For the latest dwarfs taken with both UKIRT and Subaru, the shapes of the spectra are similar for both observations, and most of the measured equivalent widths and band strengths are within the observational uncertainties.

4. Discussion

4.1. Identification as YSOs Using the Bγ Feature

We identified 12 sources as YSOs, whose Bγ feature is in emission or in flat (featureless). We regard a featureless spectrum around the Bγ line with an uncertainty of less than 2 Å in equivalent width as flat. The line emission is probably due to the accretion of matter from the circumstellar disk onto the star (e.g. Najita et al. 1996).

The other 11 objects with Bγ absorption are, on the other hand, likely to be early-type field-stars. The equivalent widths of the Bγ absorption feature are 4 Å–15 Å, consistent with the spectral types of B, A, and early F (Ali et al. 1995). Their locations on the color–color diagram are close to that of early-type field stars. Figure 3 shows the color–color diagram of the YSO candidates and field stars identified by ITG toward Heiles Cloud 2. The objects with the Bγ absorption tend to be located near the boundary between the "YSO region" and the "field-star region". Therefore, these objects may be early-type field-stars and have been misidentified as YSO candidates by photometric classification. The star-count model of Jones et al. (1981) predicts 9 B- and A-type stars for $K < 12$ in a $1^\circ \times 1^\circ$ region toward Heiles Cloud 2. This predicted number is consistent with the observational number of early type stars. Note that the number of such early-type stars does not increase for $K > 12$ toward the high-latitude direction, such as the Taurus molecular cloud.

The uncertainty in the slope of the reddening vector may also account for the misidentification. For the Taurus molecular cloud, the smallest value of $E(J-H)/E(H-K)$ is 1.58 (Elias 1978), whereas the highest is 2.0 (Gomez et al. 1994). From photometric study alone, the identification of YSOs depends on the extinction law, especially for objects near the boundary between the YSO region and the field star region on the color–color diagram.

4.2. Effective Temperature

We first describe the possible K-band features with which the effective temperatures of the M dwarfs and giants are derived. We then apply this method to the YSOs to derive their effective temperatures.

For cooler objects the conversion from MK spectral type to effective temperature is not straightforward because models do not exist to give the spectral type vs. effective temperature for pre–main-sequence stars. Because the YSOs have a luminosity class between dwarfs and giants, as we discuss below, we use the conversions for both dwarfs and giants. In this paper we have adopted the conversions given by Tokunaga (2000) both for dwarfs and giants, Bessell (1991) for late M dwarfs, and Fluks et al. (1994) for late M giants. As can be seen in figure 4, the difference in effective temperature is as much as

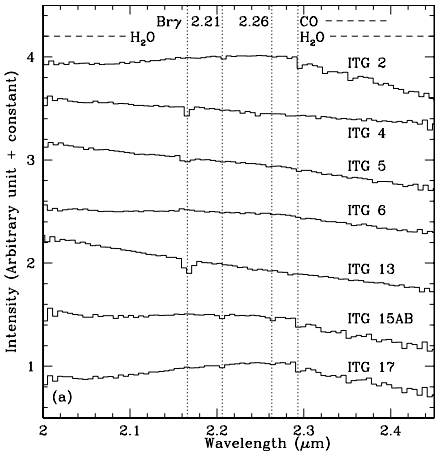

Fig. 1. (a) K-band spectra of the YSO candidates taken with UKIRT. The spectra were normalized by the flux between 2.18 μm and 2.20 μm, then offset in steps of 0.5.

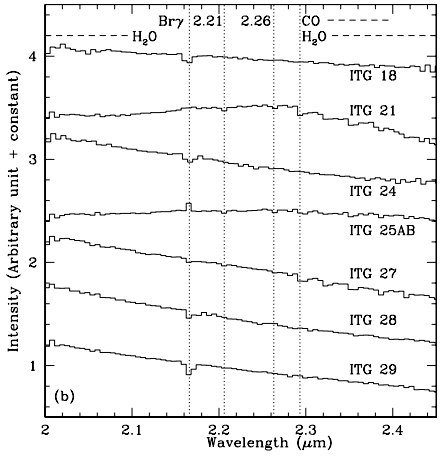

Fig. 1. (b) K-band spectra of YSO candidates taken with UKIRT. The spectra are offset in steps of 0.5.

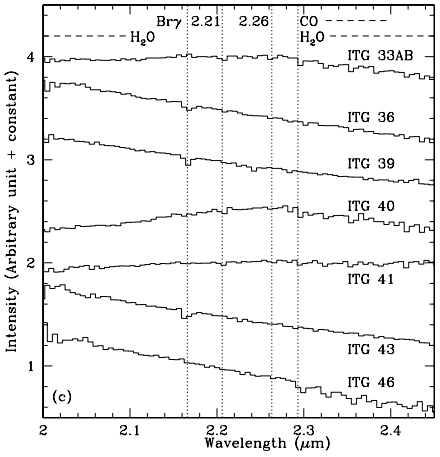

Fig. 1. (c) K-band spectra of YSO candidates taken with UKIRT. The spectra are offset in steps of 0.5.

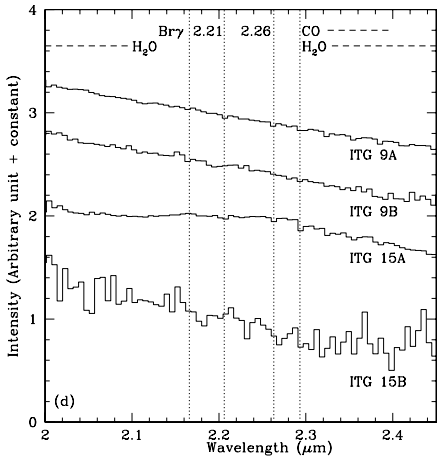

Fig. 1. (d) K-band spectra of YSO binary candidates taken with Subaru. Additive constants for the spectra are 0, 1, 1.5, and 2, respectively.

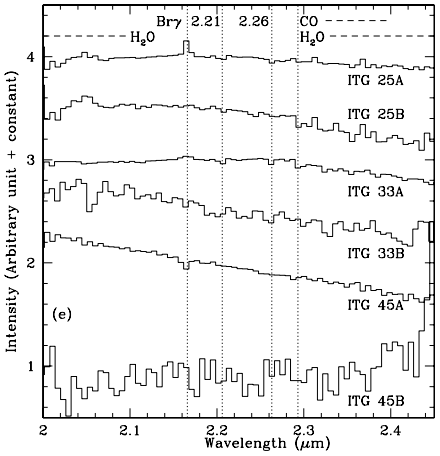

Fig. 1. (e) K-band spectra of YSO binary candidates taken with Subaru. Additive constants are 0, 1, 1.5, 2, 2.5, and 3.

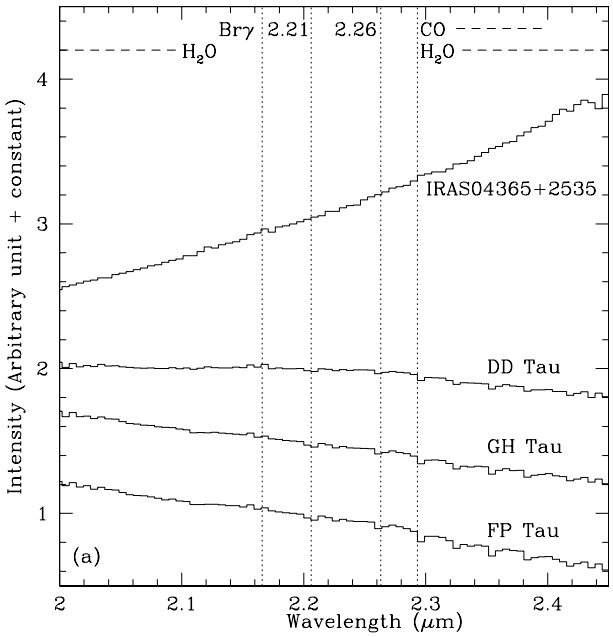

Fig. 2. (a) *K*-band spectra of CTTSs and a protostar taken with UKIRT. The spectra are normalized by the flux between 2.18 μm and 2.20 μm. Additive constants for the spectra are 0, 0.5, 1, and 2, respectively.

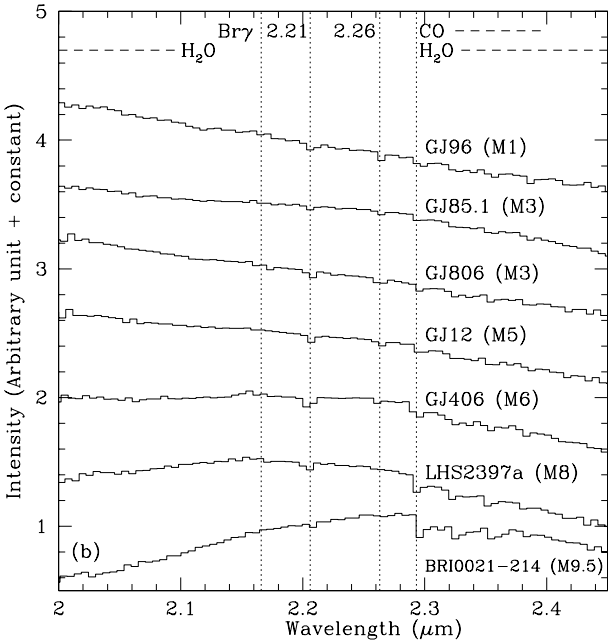

Fig. 2. (b) The *K*-band spectra of late-type dwarfs taken with UKIRT. The spectra are offset in steps of 0.5.

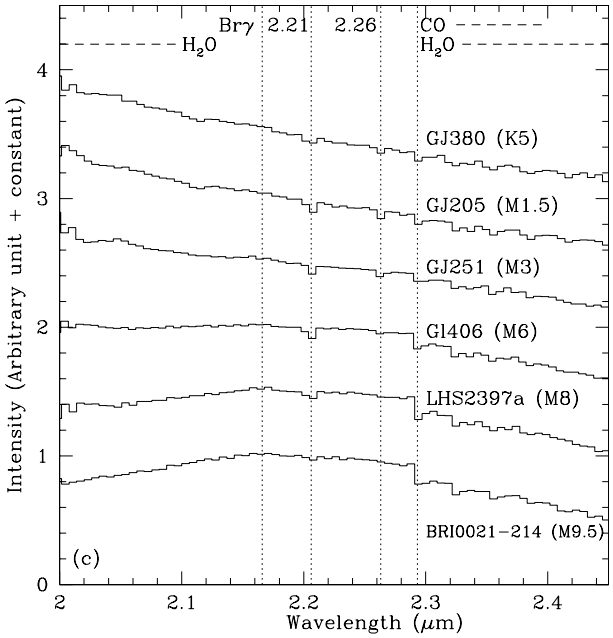

Fig. 2. (c) *K*-band spectra of late-type dwarfs taken with Subaru. The spectra are offset in steps of 0.5.

800 K between M dwarfs and M giants, even for the same spectral type.

4.2.1. 2.21-μm feature

The 2.21-μm feature consists mainly of Na, Sc, Si, and V absorption lines for late-type objects (Ramírez et al. 1997). The low excitation energy of these lines makes it a strong absorption feature in M-type stars. Figure 5 shows the equivalent widths of the 2.21-μm feature of dwarfs and giants as a function of the effective temperature. The equivalent widths increase with decreasing effective temperature. Moreover, dwarfs have larger equivalent widths than giants

Table 2. Equivalent widths of the features and strengths of the band of YSO candidates, the CTTSs, and the M dwarfs.

Object	Bγ [Å]	2.21 μm [Å]	2.26 μm [Å]	CO (2–0) [Å]	CO (4–2) [Å]	Q	Obs.*	S/N
ITG 2	0.0 ± 0.8	2.18 ± 0.39	1.00 ± 0.16	6.20	7.80	0.51 ± 0.00	U	70
ITG 4	6.80 ± 0.25	0.0 ± 0.3	0.0 ± 0.1	···	···	0.98 ± 0.01	U	90
ITG 5	4.24 ± 1.50	0.80 ± 0.26	1.44 ± 0.28	2.71	1.97	0.83 ± 0.01	U	90
ITG 6	-2.25 ± 0.62	0.98 ± 0.23	0.53 ± 0.22	2.30	3.79	0.81 ± 0.01	U	90
ITG 9A	0.0 ± 0.5	2.42 ± 0.04	2.38 ± 0.08	3.45	4.72	0.89 ± 0.02	S	300
ITG 9B	0 ± 3	0 ± 3	0.0 ± 0.2	2.71	2.35	0.88 ± 0.09	S	60
ITG 13	14.08 ± 0.70	0.0 ± 0.3	0.0 ± 0.4	···	···	0.94 ± 0.01	U	60
ITG 15A&B	-0.79 ± 0.79	3.29 ± 1.00	4.12 ± 1.24	6.73	10.39	0.64 ± 0.01	U	80
ITG 15A	-3.93 ± 1.08	3.29 ± 0.24	3.19 ± 0.30	5.88	9.79	0.61 ± 0.00	S	460
ITG 15B	0.0 ± 2.5	3.53 ± 2.92	14.19 ± 12.37	25.90	26.40	$1.65^{+1.41}_{-0.82}$	S	9
ITG 17	0.0 ± 0.5	1.96 ± 0.37	2.48 ± 0.17	6.79	10.02	0.57 ± 0.01	U	30
ITG 18	8.25 ± 0.62	0.0 ± 0.3	0.0 ± 0.3	···	···	0.98 ± 0.01	U	80
ITG 21	-3.8 ± 3.8	2.22 ± 0.78	2.31 ± 0.44	5.11	8.50	0.54 ± 0.01	U	70
ITG 24	6.60 ± 1.69	0.0 ± 0.5	0.58 ± 0.12	···	···	1.03 ± 0.01	U	40
ITG 25A&B	-5.34 ± 0.91	1.94 ± 0.51	2.54 ± 0.50	3.72	5.43	0.87 ± 0.03	U	100
ITG 25A	-12.63 ± 0.22	3.38 ± 0.16	2.26 ± 0.08	3.52	8.26	0.89 ± 0.02	S	290
ITG 25B	0.0 ± 3.4	1.41 ± 0.60	2.53 ± 1.13	9.61	21.31	0.73 ± 0.09	S	60
ITG 27	0.0 ± 1.2	1.36 ± 0.64	1.33 ± 0.70	7.87	8.50	0.86 ± 0.01	U	100
ITG 28	5.52 ± 0.72	0.75 ± 0.15	0.0 ± 0.4	···	···	1.00 ± 0.01	U	50
ITG 29	11.54 ± 0.80	0.47 ± 0.12	0.0 ± 0.1	···	···	0.96 ± 0.01	U	65
ITG 33A&B	-2.83 ± 1.05	3.68 ± 0.43	3.76 ± 0.37	6.16	8.56	0.74 ± 0.01	U	55
ITG 33A	-5.85 ± 0.85	3.78 ± 0.54	3.92 ± 0.47	6.02	7.35	0.73 ± 0.01	S	660
ITG 33B	0.0 ± 2.9	7.54 ± 4.90	···	0 ± 9	···	0.90 ± 0.04	S	20
ITG 36	5.14 ± 1.63	1.20 ± 0.43	1.26 ± 0.33	···	···	0.91 ± 0.01	U	50
ITG 39	7.40 ± 0.70	0.0 ± 0.2	0.0 ± 0.2	···	···	1.00 ± 0.02	U	60
ITG 40	0.0 ± 0.9	4.15 ± 1.00	1.78 ± 0.53	4.95	10.76	0.67 ± 0.02	U	30
ITG 41	0.0 ± 1.0	2.31 ± 0.50	2.08 ± 0.56	3.43	6.53	0.93 ± 0.01	U	100
ITG 43	7.68 ± 0.98	0.0 ± 0.4	0.0 ± 0.2	···	···	0.97 ± 0.01	U	60
ITG 45A	8.26 ± 0.96	0.0 ± 0.88	0.0 ± 1.8	···	···	0.88 ± 0.07	S	80
ITG 45B	0 ± 25	0 ± 4	0 ± 9	···	···	$1.55^{+1.77}_{-0.83}$	S	6
ITG 46	0.0 ± 1.0	1.46 ± 0.50	1.34 ± 0.33	11.13	13.69	0.80 ± 0.01	U	70
DD Tau (M1)	-2.53 ± 0.35	1.99 ± 0.42	1.84 ± 0.25	3.21	4.93	0.82 ± 0.01	U	100
GH Tau (M2)	-0.58 ± 0.57	2.91 ± 0.46	2.81 ± 0.48	5.01	6.92	0.85 ± 0.01	U	130
FP Tau (M5.5)	-1.02 ± 0.46	3.35 ± 0.69	3.47 ± 0.38	6.91	8.27	0.75 ± 0.00	U	150
IRAS 04365+2535	-1.68 ± 0.94	0.0 ± 0.2	0.0 ± 0.2	···	···	1.06 ± 0.02	U	160
GJ 380 (K5)	-0.14 ± 0.25	4.20 ± 0.19	4.14 ± 0.25	6.28	9.56	0.93 ± 0.01	S	630
GJ 96 (M1)	-1.80 ± 1.80	4.78 ± 1.18	4.24 ± 0.24	6.67	7.19	0.84 ± 0.01	U	110
GJ 205 (M1.5)	0.00 ± 0.47	7.16 ± 0.51	5.80 ± 0.30	4.37	8.31	0.87 ± 0.01	S	780
GJ 85.1 (M3)	-1.04 ± 0.74	2.60 ± 0.60	1.97 ± 0.39	3.74	5.11	0.66 ± 0.01	U	310
GJ 806 (M3)	-0.40 ± 0.40	4.08 ± 0.34	3.97 ± 0.36	4.88	7.39	0.81 ± 0.01	U	100
GJ 251 (M3)	0.0 ± 0.1	5.67 ± 0.47	4.01 ± 0.20	4.90	8.08	0.77 ± 0.01	S	620
GJ 12 (M5)	0.0 ± 0.7	4.39 ± 0.34	3.37 ± 0.27	···	···	0.71 ± 0.01	U	60
GJ 406 (M6)	-1.72 ± 0.76	7.67 ± 0.75	1.65 ± 0.15	8.13	7.96	0.55 ± 0.01	U	60
GJ 406 (M6)	0.0 ± 0.1	7.23 ± 0.31	2.10 ± 0.95	6.02	7.35	0.60 ± 0.00	S	510
LHS 2397a (M8)	0.0 ± 0.7	4.98 ± 0.31	0.39 ± 0.07	14.32	13.54	0.51 ± 0.01	U	90
LHS 2397a (M8)	-2.10 ± 1.19	5.04 ± 0.15	0.24 ± 0.24	11.44	12.79	0.51 ± 0.01	S	420
BRI 0021−214 (M9.5)	0.0 ± 0.3	2.87 ± 0.52	1.75 ± 0.82	11.54	10.59	0.52 ± 0.01	U	70
BRI 0021−214 (M9.5)	0.0 ± 0.6	2.98 ± 0.26	0.05 ± 0.02	9.57	7.60	0.49 ± 0.01	S	200

* U: UKIRT, S: Subaru.

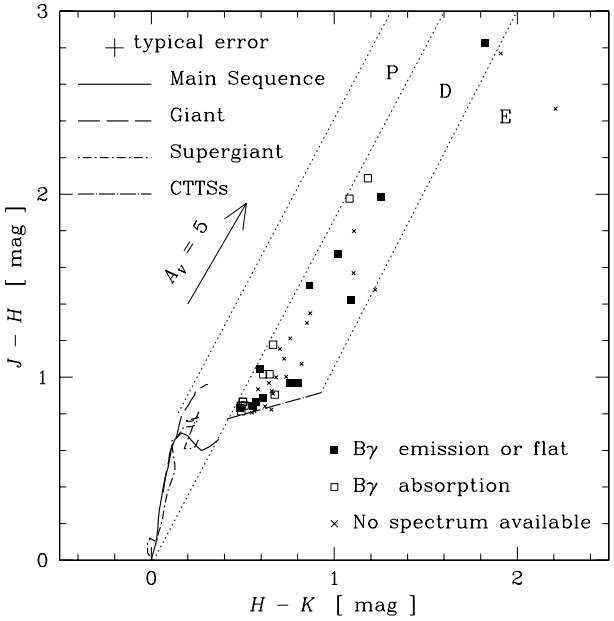

Fig. 3. Color–color diagram for Heiles Cloud 2. The intrinsic colors of main-sequence stars, giants (Bessell, Brett 1988), supergiants (Tokunaga 2000), and CTTSs (Meyer et al. 1997) are plotted with the reddening vector (Koornneef 1983; $E(J-H)/E(H-K) = 1.7$ in the CIT system). All colors are transformed to the Johnson/Glass system (Bessell, Brett 1988). Following the scheme discussed by Strom et al. (1993), the near-infrared sources are classified into three groups. In the "P" (photosphere) region on the color–color diagram, located are main sequence stars, giants, weak-line T Tauri stars objects, and the CTTSs whose near-infrared excess is small. In the "D" (disk) region, a part of CTTSs are located. Protostars are located in the "E" (envelope) region on the color–color diagram. The objects located in the "D" region or the "E" region were identified as YSO candidates by a previous photometric study (ITG). The objects without absorption (i.e. with emission or in flat) in the Bγ line are denoted by filled squares, as well as the objects with absorption by open squares. The YSO candidates without the spectroscopic observations are plotted by crosses. Field stars identified by ITG are shown by dots.

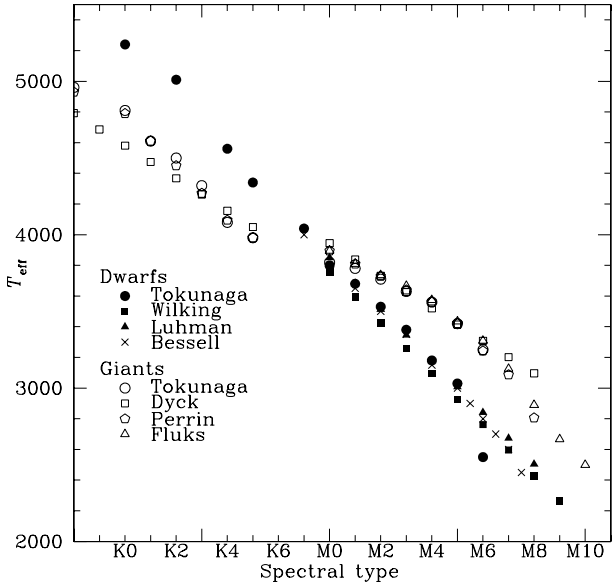

Fig. 4. Relation between the effective temperature and spectral type for dwarfs and giants. The data were taken from Tokunaga (2000), Wilking et al. (1999), Luhman and Rieke (1998), Bessell (1991), Dyck et al. (1998), Perrin et al. (1998), and Fluks et al. (1994).

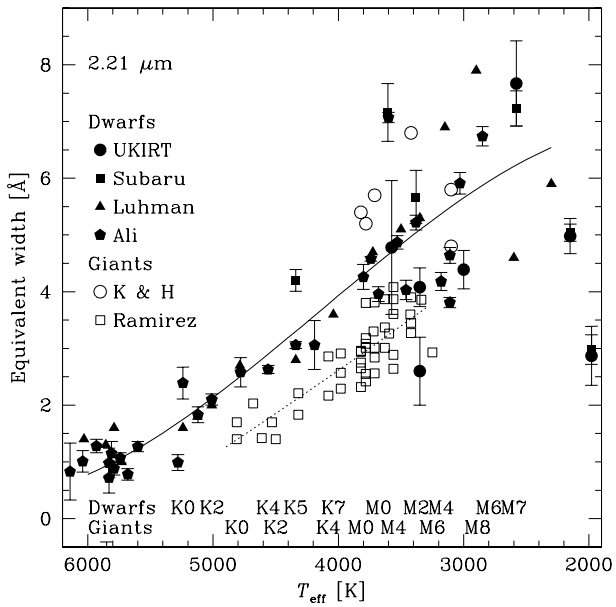

Fig. 5. Equivalent widths of the 2.21-μm feature as a function of effective temperature. The data were taken from Luhman and Rieke (1998), Ali et al. (1995), Kleinmann and Hall (1986), Ramírez et al. (1997), and this paper. The filled symbols represent the equivalent widths for dwarfs and the open symbols for giants. The solid line shows a fitted line for dwarfs with $T_{\rm eff} > 2300$ K, and the dotted line for giants listed in Ramírez et al. (1997).

at the same effective temperature. The 2.21-μm feature has, therefore, a strong dependence on the effective temperature and a weak dependence on gravity (Kleinmann, Hall 1986; Terndrup et al. 1991; Ramírez et al. 1997).

Near-infrared Na lines of CTTSs have a symmetric profile, indicating photospheric origin (Greene, Lada 1997), while optical Na lines are red-shifted, indicating outflow origin (Gullbring et al. 1996).

4.2.2. 2.26-μm feature

The 2.26-μm feature consists mainly of Ca, Si, and Ti lines for late-type objects (Ramírez et al. 1997). Figure 6 shows the equivalent widths of the 2.26-μm feature of dwarfs and giants as a function of the effective temperature. The 2.26-μm feature has a peak in its equivalent width around 3500 K; its width then decreases with decreasing temperature, due to the moderate excitation energy of Ca. This feature also has a strong dependence on the effective temperature, and a weak dependence on gravity (Ramírez et al. 1997).

4.2.3. Ratio of metallic features

The use of the ratio of the feature strengths to derive the effective temperature can avoid not only the effect of metallicity, but also the effect of veiling if features whose wavelengths are close to each other are selected (Meyer 1996). We have

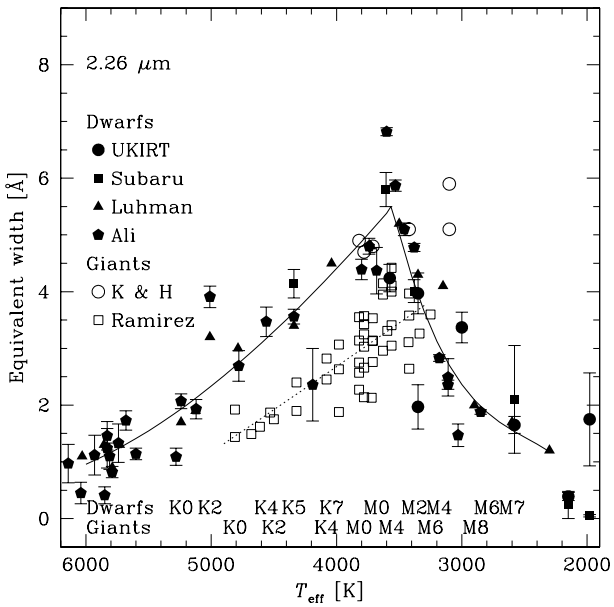

Fig. 6. Equivalent width of the 2.26-μm feature as a function of the effective temperature. The filled symbols represent the equivalent widths for dwarfs and the open symbols for giants. The solid lines show fitted lines for dwarfs, and the dotted line for giants listed in Ramírez et al. (1997). The intensity has a peak at 3500 K for dwarfs.

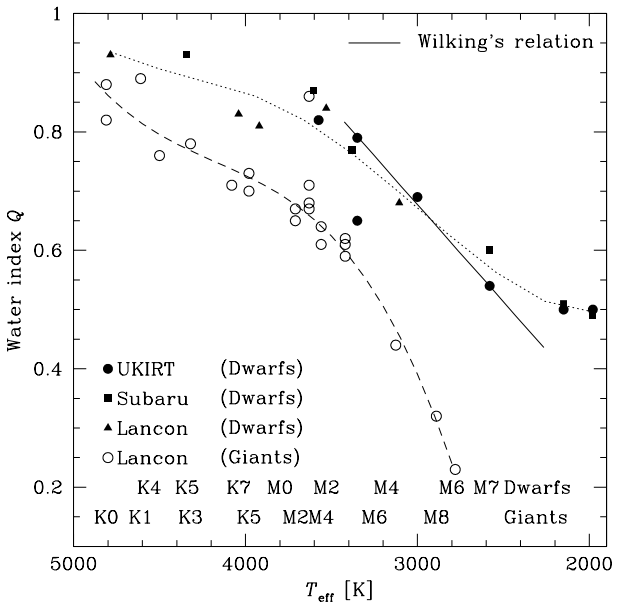

Fig. 8. Q index as a function of the effective temperature. The data are taken from our observations and from Lançon and Rocca-Volmerange (1992). The solid line shows the relationship between the Q indices and the spectral type for dwarfs (Wilking et al. 1999). The dotted line shows a fitted line of the Q index for the dwarfs, and the dashed line for the giants.

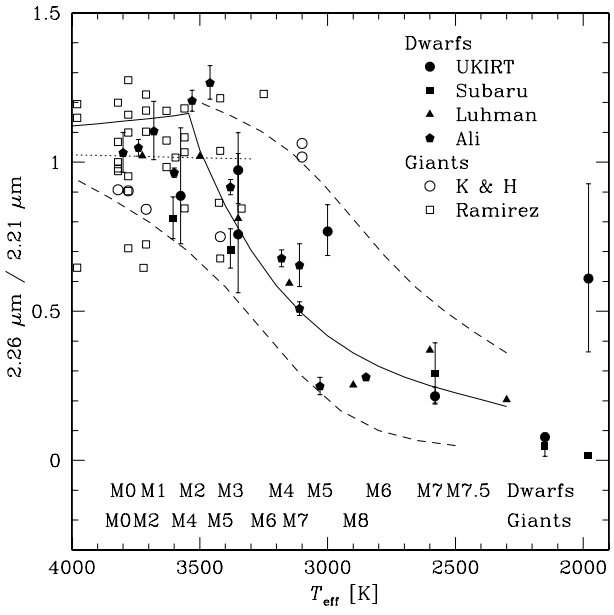

Fig. 7. Ratio of the 2.26-μm feature to the 2.21-μm feature as a function of the effective temperature. Data are taken from our UKIRT observations, Subaru observations, Luhman and Rieke (1998), Ali et al. (1995), Kleinmann and Hall (1986), and Ramírez et al. (1997). The solid lines show the ratio for dwarfs, and the dotted line for giants, both derived from the fitted lines in figures 5 and 6. The dashed lines show the conversions used for estimate of the upper limit and the lower limit of the effective temperature of the YSOs.

checked whether the 2.21-μm feature and the 2.26-μm feature can be used as a ratio index of the effective temperature. Figure 7 shows the 2.26-μm/2.21-μm feature ratio for dwarfs and giants as a function of the effective temperature. Although the scattering is relatively large and no data is available for cool giants, the ratio decreases as the temperature decreases. Because dwarfs and giants have similar values, the surface gravity does not appear to significantly affect this feature ratio. Therefore, this feature ratio is a sensitive indicator of the effective temperature for $T_{\rm eff} < 3300$ K. For 2.26 μm/2.21 μm > 1, only lower limits of the effective temperature can be estimated.

4.2.4. H_2O

The H_2O absorption bands in the near-infrared wavelengths are a sensitive function of the effective temperature for cool stars (Aaronson et al. 1978; Jones et al. 1994). Figure 8 shows the water index, Q, of the dwarfs taken from our observations, as well as those of dwarfs and giants taken from Lançon and Rocca-Volmerange (1992). The dotted line represents a fitted line of the Q index for the dwarfs and the dashed line for the giants. In this figure, the relation between the Q index and spectral type for M dwarfs derived by Wilking et al. (1999), also shown by the solid line. While Wilking's relation is consistent with the plotted Q indices for the dwarfs; the Q indices for giants are much smaller than Wilking's relation. Since the YSOs have surface gravity between dwarfs and giants, as we discuss below, we should use both the relation for the dwarfs and that for the giants to estimate the effective temperature of the YSOs. Note that the veiling effect by a circumstellar disk could increase the Q index, leading to higher temperatures.

Table 3. Effective temperatures and spectral types of the YSOs and the CTTSs.

Object	$T_{\rm eff}$(ratio)* [K]	$T_{\rm eff}$(2.21)† [K]	$T_{\rm eff}$(2.26)‡ [K]	$T_{\rm eff}$(Q)§ [K]	$T_{\rm eff}$(NIR)‖ [K]	$T_{\rm eff}$(Opt)# [K]	Sp.(V)**	Sp.(III)††	$\log L_{\rm bol}$‡‡ [$L_\odot$]
ITG 2	2300–3400	< 5200	···	2400–3200	2400–3200		M4–M8	> M6	−1.11– − 0.81
ITG 4	field-star								
ITG 5	field-star								
ITG 6	2300–3700	···	···	3500–3700	3500–3700		M1–M2	M2–M4	−1.72– − 1.42
ITG 9A	> 3000	···	···	> 3700	> 3700		< M1	< M1	
ITG 9B	···	···	···	> 3600	> 3600		< M2	< M4	
ITG 13	field-star								
ITG 15A&B	> 3000	< 4800	< 4700	3000–3600	3000–3600		M2–M5	M4–M7.5	−0.95– − 0.65
ITG 15A	> 3000	···	···	2900–3500	3000–3500		M2–M5	M5–M7.5	−0.95– − 0.65
ITG 15B	> 3100	···	···	···	···		···	···	
ITG 17	···	···	···	2700–3400	2700–3400		M3–M6.5	> M5	−1.49– − 1.19
ITG 18	field-star								
ITG 21	> 2900	···	···	2600–3200	2900–3200		M4–M5	M6–M7.5	−1.36– − 1.06
ITG 24	field-star								
ITG 25A&B	> 3250	···	···	3600–4800	3600–4800		K3–M1	K0–M2	−0.69– − 0.39
ITG 25A	2700–3600	···	···	> 3700	2700–3600		M2–M6.5	M4–M8	−0.57– − 0.27
ITG 25B	···	···	···	2900–4400	2900–4400		K5–M5	K3–M8	−2.23– − 1.93
ITG 27	>2500	···	···	3600–4800	3600–4800		K3–M1	K0–M2	−0.44– − 0.14
ITG 28	field-star								
ITG 29	field-star								
ITG 33A&B	> 3200	< 4400	< 4400	3300–4100	3300–4100		K7–M3	K4–M6	−2.02– − 1.72
ITG 33A	···	···	···	3200–4000	3200–4000		M0–M4	M0–M6	−2.02– − 1.72
ITG 33B	···	···	···	> 3700	> 3700		< M1	< M0	
ITG 36	field-star								
ITG 39	field-star								
ITG 40	2000–3400	< 4400	···	3000–3700	3000–3400		M3–M5	M5–M7.5	−1.50– − 1.20
ITG 41	> 2750	···	···	> 3800	> 3800		< M0	< M0	
ITG 43	field-star								
ITG 45A	field-star								
ITG 45B	···	···	···	> 3200	> 3200		< M4	< M6	
ITG 46	> 2700	···	···	3500–4500	3500–4500		K4–M2	K2–M4	−1.63– − 1.33
DD Tau	> 2900	···	···	3500–4500	3500–4500	3700–3900	K4–M2	K2–M4	
GH Tau	> 2900	< 4800	···	3600–4800	3600–4800	3500–3700	K3–M2	K0–M4	
FP Tau	> 3100	< 4700	< 5000	3300–4100	3300–4100	2900–3700	K7–M3	K4–M6	

* $T_{\rm eff}$ estimated from the 2.26-μm/2.21-μm feature ratio.
† $T_{\rm eff}$ estimated from the the equivalent widths of the 2.21-μm feature. Because YSOs are subject to continuum emission and the strength of the line increases with lower temperature, only the upper limit of the effective temperature can be estimated.
‡ $T_{\rm eff}$ estimated from the equivalent widths of the 2.26-μm feature.
§ $T_{\rm eff}$ estimated from the Q index. The range of temperatures for $T_{\rm eff}$(Q) includes estimates for both dwarf and giant surface gravities. These effective temperatures may be upper limits, due to veiling effect.
‖ $T_{\rm eff}$ estimated from the 2.26-μm/2.21-μm feature ratio and the Q index.
$T_{\rm eff}$ converted from optical spectral type.
** Estimated spectral type in the dwarf scale.
†† Estimated spectral type in the giant scale.
‡‡ Bolometric luminosity for the midpoint of $T_{\rm eff}$ (NIR), estimated from the previous photometric study (see subsubsection 4.4.1).

4.2.5. Effective temperatures of YSOs

The effective temperatures of the observed YSOs and their companions were derived using the 2.26-μm/2.21-μm feature ratio and the Q index [$T_{\rm eff}$ (NIR) in table 3]. The effective temperatures of most YSOs are less than 4000 K, lower than that of typical CTTSs.

The effective temperatures of the observed CTTSs are also derived from the near-infrared features. The effective temperatures estimated from the near-infrared spectroscopy are consistent with those converted from optical spectral types for all of the CTTSs.

4.3. Luminosity Class

Since the 2.21 μm feature and the 2.26 μm feature are primarily sensitive to the effective temperature, and the depth of the CO band varies with the surface gravity, the luminosity

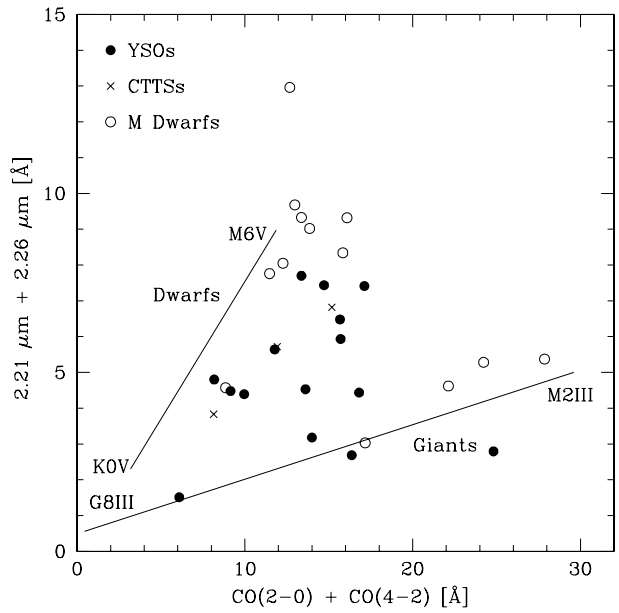

Fig. 9. Luminosity class of the YSOs. The combined equivalent width of the 2.21-μm feature and the 2.26-μm feature is plotted against the combined CO band equivalent width. Loci of dwarfs and giants (Greene, Meyer 1995) are shown by the solid lines.

class of the object is estimated from a plot of the equivalent widths of these atomic features against the widths of the CO band. Figure 9 shows the sum of the equivalent widths of the 2.21-μm feature and the 2.26-μm feature against the CO band equivalent width of the YSOs, the CTTSs, and the late-type dwarfs. The sum of the equivalent widths of the CO (2–0) and CO (4–2) bands is used as a CO equivalent width. The CO (3–1) band is not included because it contains a sodium line (Kleinmann, Hall 1986). The relationships for giants and dwarfs (Greene, Meyer 1995) are also shown in the figure by the solid lines. Their fits are only applied to stars with spectral types $<$ M6 V and $<$ M2 III, and cannot be applied to very late-type stars. Points of very late-type dwarfs are close to the line for giants, since their equivalent width of the 2.26-μm feature diminishes (see figure 6).

Most of the YSOs lie, like the CTTSs, between these two lines. Therefore, most of the YSOs and the CTTSs have a luminosity class between dwarfs and giants, classified as luminosity class IV.

4.4. Mass and Age of the YSOs

Based on the effective temperature described above and the bolometric luminosity described below, the masses of the YSOs and their companions are estimated with recent evolutionary tracks on the HR diagram.

4.4.1. Bolometric luminosity

The bolometric luminosity of the YSOs is estimated from the J-band luminosity, because the J-band emission arises primarily from the photosphere of YSOs (Bertout et al. 1988). First, the J-band luminosity of the YSOs is corrected for interstellar extinction on the color–color diagram (ITG). Next, three cases are assumed, where the fraction of the photospheric luminosity to the total luminosity is 1.0, 0.8, and 0.5 in the J-band. Then, by comparing the photospheric luminosity of the YSOs with that of late-type dwarfs in the J-band (Leggett et al. 1996), the bolometric luminosity of the YSO's photosphere is estimated.

This procedure has the following uncertainties:

1. The extinction of each YSO is corrected on the color–color diagram. If the extinction law of Bessell and Brett (1988) is used instead of Koornneef (1983), a 6% larger value is derived as visual extinction, making the intrinsic luminosity brighter by about 2%.
2. The extinction is deduced from the distance between the observed color of the object and the intrinsic color of CTTSs on the color–color diagram. The intrinsic color of CTTSs deduced by Meyer et al. (1997) has a dispersion of as much as 0.17 mag in $J-H$, corresponding to an uncertainty of 1.5 mag in visual extinction or 0.16 dex in bolometric luminosity.
3. The intrinsic color of YSOs might be different from the intrinsic color of CTTSs. The central objects of the YSOs are M-type stars, whereas those of CTTSs are mainly K-type stars. The color of an M-type dwarf is about 0.1 mag redder than that of a K-type dwarf both in $J-H$ and $H-K$.
4. We assumed that the distance to the Taurus molecular cloud is 140 pc. Hipparcos observations estimate 142 pc with an uncertainty of $\pm$14 pc as the distance to the cloud (Wichmann et al. 1998). Therefore, the uncertainty due to distance is $\pm$0.1 dex in bolometric luminosity.
5. The fractions of the photospheric luminosity are assumed to be 1.0, 0.8, and 0.5 of the total luminosity in the J-band. In these three cases, the uncertainty is 0.3 dex in bolometric luminosity. If the fraction is smaller, the photospheric luminosity is fainter. Although the fraction value could be deduced from the veiling effect index, r_J (Greene, Meyer 1995), r_J has a large uncertainty for all YSOs due to rather large observational uncertainties in the equivalent widths of the metallic features. Therefore, we did not employ r_J to estimate the photospheric luminosity.

4.4.2. HR diagrams

Several groups have recently developed and refined evolutionary tracks for low-mass stars, brown dwarfs, and even giant planets. Figures 10, 11, and 12 show the HR diagrams of the YSOs and their companions. Overlaid are the evolutionary tracks of D'Antona and Mazzitelli (1994, 1997) and Baraffe et al. (1998).

The mass and age for individual YSOs are estimated from the HR diagrams with the evolutionary tracks (table 4). Some YSOs are indeed very low-mass YSOs (typically 0.1 $M_\odot$–0.3 $M_\odot$). These objects are definitively a *different population* from the CTTSs in terms of their mass. The uncertainties in the mass are about a factor of 2, and those in the age are about a factor of 5 for the YSOs, as shown in the figures. On the other hand, neither the mass nor the age of the companions was determined, mainly due to the poor signal-to-noise ratio on the spectra. Additional notes are given in the appendix for most companions.

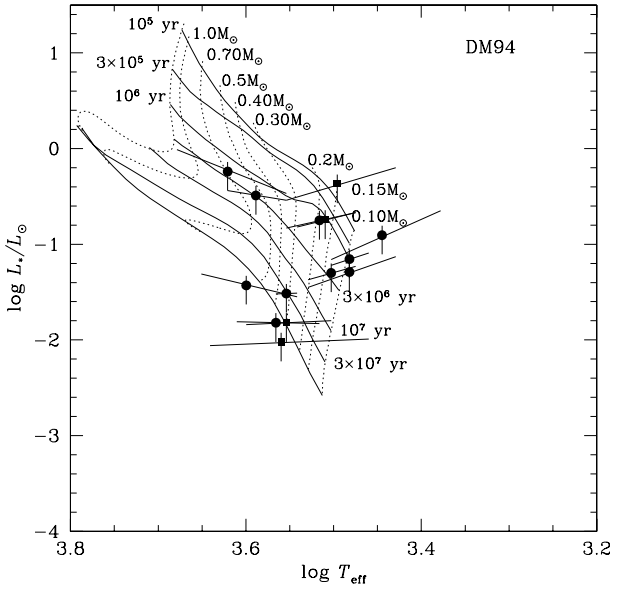

Fig. 10. HR diagram of YSOs with the evolutionary tracks of D'Antona and Mazzitelli (1994) with the Alexander opacities and the CM convection overlaid. The filled circles and filled squares show the loci of the YSOs deduced from the UKIRT observations and from the Subaru observations, respectively. $T_{\rm eff}$ (NIR) in table 3 are adopted. The error bars are tilted, because the bolometric luminosity is a function of the J-band luminosity and the effective temperature (see subsubsection 4.4.1).

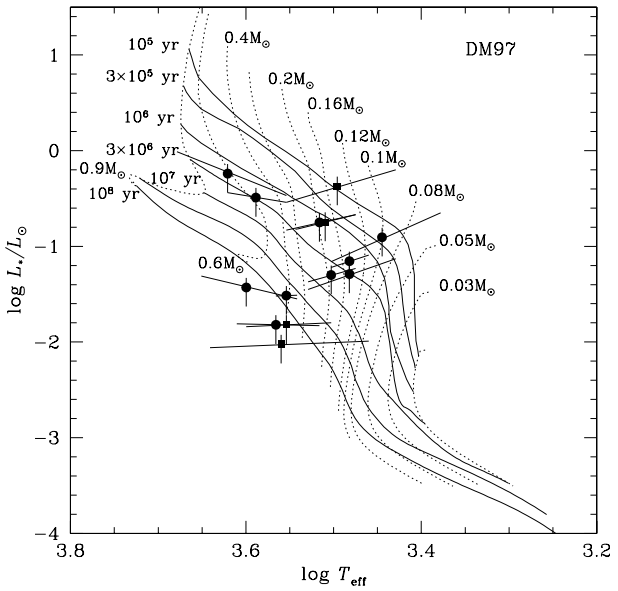

Fig. 11. HR diagram of YSOs with evolutionary tracks of D'Antona and Mazzitelli (1997) overlaid.

The mass–luminosity relation of the YSOs is shown in figure 13; also shown are the mass–luminosity relations of CTTSs (Strom et al. 1989) and the predicted relations for three ages calculated from Baraffe et al. (1998). Most of the YSOs are distributed within one order of magnitude in the ages. Both CTTSs and the YSOs have near-infrared excesses, implying the existence of circumstellar disks. The ages of these objects

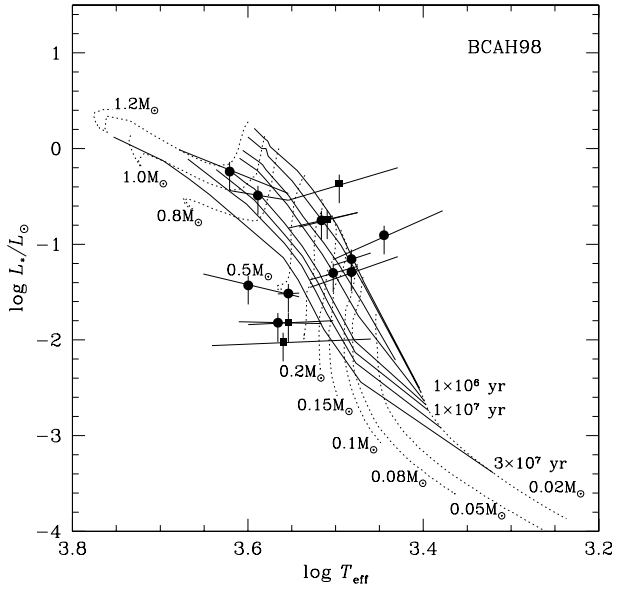

Fig. 12. HR diagram of YSOs with evolutionary tracks of Baraffe et al. (1998) overlaid.

indicate the survival time of the circumstellar disk; it is interesting to ask whether the mass of the central object affects the evolution of the circumstellar disk. The ages of most YSOs are less than 10^7 yr, similar to the ages of the CTTSs. However, since the mass–age relation of YSOs depends strongly on evolutionary tracks (figures 10, 11, 12, and table 4), we cannot conclude that the disk survival time is independent of the mass of the central object.

The small amount of objects prevents us from making a mass function of the YSOs. In the four other regions, except for Heiles Cloud 2, Luhman (2000) shows that the mass function has a peak at 0.8 $M_\odot$, and is relatively flat between 0.1 $M_\odot$ and 0.8 $M_\odot$. Briceño et al. (1998) as well as Luhman (2000) suggest a deficit of brown dwarfs in the regions, although Martín et al. (2001) have identified four brown dwarfs in two sparsely populated stellar groups. Given the limiting magnitude of the ITG survey ($K = 13.4$) and an age of 1 Myr, we expect to reach a mass limit of 0.03 $M_\odot$ for $A_V = 0$ with the survey. In order to take a census of brown dwarfs in Heiles cloud 2 and to construct an initial mass function of the cloud, a deeper spectroscopic search is required.

4.5. Comparison with Other Studies

Wilking et al. (1999) carried out K-band spectroscopic observations of low-luminosity sources in the ρ Oph cloud. They estimated the spectral types of the objects using the Q index, then derived the effective temperatures using the conversion for dwarfs. The effective temperature derived from their method is the same as the lower limit of the effective temperatures derived from the Q index in this paper. This is because M giants have a higher temperature than M dwarfs, even with the same Q index, due to the gravity dependence of the water band depth (see figure 8). For example, ITG 40 has a Q of 0.67, which corresponds to a spectral type of M4.7 for Wilking's relation. This spectral type corresponds to 2980 K in the dwarf scale, which

Table 4. Mass and age of the YSOs.

Object	DM 94*		DM 97†		BCAH 98‡	
	mass $[M_\odot]$	age $[10^6\,\mathrm{yr}]$	mass $[M_\odot]$	age $[10^6\,\mathrm{yr}]$	mass $[M_\odot]$	age $[10^6\,\mathrm{yr}]$
ITG 2	< 0.15	< 2	0.05–0.18	< 3	< 0.2	< 3
ITG 6	0.25–0.4	20–50§	0.35–0.45	> 30§	0.4–0.5	> 50§
ITG 15A&B	0.1–0.4	0.1–3	0.12–0.4	0.2–5	< 0.55	< 8
ITG 15A	0.1–0.3	0.1–3	0.12–0.3	0.2–4	< 0.45	< 5
ITG 17	< 0.2	< 10	0.08–0.3	0.3–20	< 0.3	< 20
ITG 21	< 0.15	< 2	0.11–0.19	1–5	< 0.2	< 4
ITG 25A&B	0.35–0.8	1–10	0.35–0.75	2–8	0.57–1.00	4–18
ITG 25A	< 0.35	< 1	0.09–0.35	< 2	< 0.57	< 4
ITG 25B	···	···	> 0.08	> 10	> 0.06	> 4.5
ITG 27	0.3–1.2	1–5	> 0.3	1–8	0.57–1.2	3–18
ITG 33A&B	> 0.15	> 10§	> 0.2	> 30§	> 0.2	> 30§
ITG 33A	> 0.15	> 10§	> 0.2	> 30§	> 0.14	> 18§
ITG 40	< 0.2	1–7	0.14–0.3	2–15	0.1–0.32	4–18
ITG 41	···	···	···	···	···	···
ITG 46	> 0.25	> 20§	> 0.35	> 30§	> 0.35	> 30§

* D'Antona and Mazzitelli (1994) with the Alexander opacities and the CM convection.
† D'Antona and Mazzitelli (1997).
‡ Baraffe et al. (1998).
§ These ages are discussed further in the appendix.

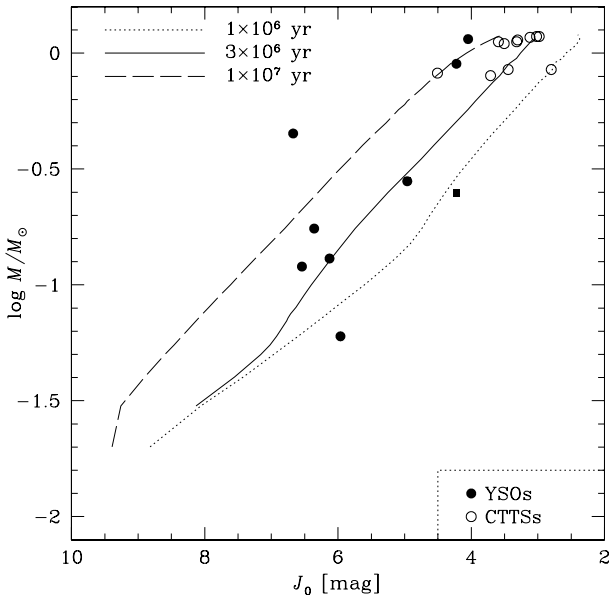

Fig. 13. Mass–absolute J-band magnitude relation of the YSOs and the CTTSs listed in Strom et al. (1989). The J-band magnitudes were corrected for interstellar extinction on the color–color diagram (ITG). The mass of the YSOs and the CTTSs are estimated from the evolutionary track of Baraffe et al. (1998). The distance modulus of the Taurus molecular cloud is 5.73 (Elias 1978).

is consistent with the lower limit on the effective temperature derived from the Q index in this paper.

They estimated the extinction of each object from the $J-H$ color, assuming no infrared excesses in the J- and H-bands. This procedure could lead to a slightly higher value for extinction than our method. For example, A_V of ITG 40 is estimated to be 20.0 mag by their method. On the other hand, our value is 16.7 mag. A larger A_V leads to higher values in bolometric luminosity. The bolometric luminosity of ITG 40 is estimated to be 0.1 $L_\odot$ by their method, whereas it is 0.05 $L_\odot$ by us, even though the discrepancy is within the uncertainty.

Luhman and Rieke (1998) carried out K-band spectroscopy of low-luminosity sources in the L 1495 cloud in Taurus. They derived the spectral type of the object by fitting the 2.21-μm feature and 2.26-μm strengths of the object to those of dwarf stars varying in amounts of veiling. With their method, the spectral type of ITG 40 is estimated to be M3 or M7. The derived spectral type corresponds to 2600 K–3400 K, in agreement with our result.

5. Conclusions

1. We carried out near-infrared spectroscopic observations of 23 very low-luminosity YSO candidates and 5 of their companions in Heiles Cloud 2 in the Taurus molecular cloud. Near-infrared spectroscopy is essential to characterize objects in the color–color diagram. Out of the 28 objects, 5 objects have Bγ in emission and 7 have "flat" spectra over the Bγ feature. We conclude that these 12 objects are indeed YSOs.
2. Compiling near-infrared spectra of dwarfs and giants taken by us as well as those in the literature, the ratio of the 2.26-μm feature to the 2.21-μm feature turns out to be a good indicator of the effective temperature for M-type stars.
3. The effective temperatures of the YSOs were determined. These objects are cool ($T_{\mathrm{eff}} < 4000$ K) YSOs.

4. The mass of these YSOs was estimated from the HR diagram with recent evolutionary tracks. Some objects are very low-mass (0.1 $M_\odot$–0.3 $M_\odot$) YSOs.
5. The ages of these YSOs appear to be 10^5–10^7 years. However, the deduced age depends on evolutionary track models.

We are grateful to T. Geballe, T. Kerr, and Y. Oasa for help with the UKIRT observations, and H. Terada, N. Kobayashi, and B. Potter for the Subaru observations. We thank T. Tsuji and T. Nakajima for discussions on spectral features of late-type stars. We also thank our referee, B. Wilking, for many helpful comments. Y. I. is supported from the Sumitomo Foundation. A part of this study was supported by the UK–Japan collaboration fund from the JSPS. The United Kingdom Infrared Telescope is operated by the Joint Astronomy Centre on behalf of the U. K. Particle Physics and Astronomy Research Council. Subaru Telescope is operated by the National Astronomical Observatory of Japan.

Appendix. Individual Objects

ITG 2

The mass of this object is estimated to be less than 0.2 $M_\odot$ by any evolutionary track, possibly a young brown dwarf. The age of this object is estimated to be less than 3×10^6.

ITG 6 (GM Tau)

Gomez et al. (1994) derived the magnitude of this star as 8.06 in the K-band, one order of magnitude brighter than the magnitude derived by ITG and by Kenyon and Hartmann (1995). If the bolometric luminosity is one order of magnitude brighter, the age of this star is estimated to be around 10^6 yr, while the mass of the star is still about 0.3 $M_\odot$.

Kenyon and Hartmann (1995) classified spectral type of this star as "continuum". Therefore, the spectrum of this object has a large amount of veiling. Since only the lower limit of the effective temperature is estimated from the Q index, the true effective temperature might be lower than that estimated here. If half of the K-band flux comes from a circumstellar disk, for example, the Q index changes from 0.81 to 0.62 and the effective temperature to 2700 K–3500 K. This value is not inconsistent with the effective temperature deduced from the ratio of the 2.26 μm feature to the 2.21 μm feature. With this temperature, the mass and the age of the object would be 0.1 $M_\odot$ and 3×10^6 yr.

ITG 9

The fact that both spectra of the binary have neither the strong metallic features nor the deep water absorption bands indicates high effective temperatures of the objects. They both might be field-stars.

ITG 15A

The effective temperatures deduced from the UKIRT observations and that from the Subaru observations are very consistent with each other.

ITG 25 (IRAS 04370+2559)

While the UKIRT observations and the Subaru observations are consistent with each other in the strength of the 2.26-μm feature as well as the Q index, there is a discrepancy in the strength of the 2.21-μm feature, resulting in a different effective temperature. Because of the higher signal-to-noise ratio in the Subaru observations than in the UKIRT observations, we use the effective temperature derived from the Subaru observations. For the Subaru observations, the effective temperatures derived from the feature ratio and from the Q index are also different. As is the case of ITG 6, the veiling effect can easily increase the Q index, leading to a higher effective temperature. Because this object is an IRAS source, indicating its young age, we believe the effective temperature derived from the feature ratio, rather than that from the Q index.

For consistency between the effective temperature derived from the feature ratio and that from the Q index, the Q index should be 0.65, which means that 70% of the K-band luminosity is not of photospheric origin, but from a circumstellar disk. If the same portion of the luminosity is due to veiling for the companion ITG 25B, the Q index of the companion is suppressed to 0.08. This very low value indicates that the effective temperature is less than 2700 K and the age is less than 1×10^6 yr, implying a low-mass brown dwarf.

ITG 33

Martín (2000) classified the primary as a T Tauri star with a spectral type of M3 and with an A_V of 3.5 mag from optical spectroscopy. The spectral type derived from near-infrared spectroscopy is M0 or M4, consistent with optical spectroscopy. Visual extinction is estimated to be 3.94 ± 0.55 from near-infrared photometry, also consistent with the optical spectroscopy. Martín (2000) proposed an edge-on disk T Tauri star, like a companion of HK Tau (Koresko 1998; Stapelfeldt et al. 1998). If so, visual extinction would be very large as much as 50 mag, like the HK Tau companion, inconsistent with A_V for ITG 33A. The location of ITG 33A is odd as a YSO in the HR diagram. The veiling effect may lead to a high effective temperature. A spectrum with a high signal-to-noise ratio is required to estimate the effective temperature from metallic features.

Martín (2000) also classified ITG 33B as a field-star from optical spectroscopy. However, their optical spectrum, as well as our near-infrared spectrum, are too noisy to classify this object as a field-star or a featureless YSO. A higher signal-to-noise ratio spectrum at optical and/or of near-infrared wavelength is required.

ITG 41 (IRAS 04385+2550)

This object is identified at optical wavelengths as Haro 6-34. Weak absorption features which may imply a large amount of veiling prevents us from estimating the effective temperature, and thus its mass and age.

ITG 45

Martín (2000) found an Hα absorption line in a spectrum of ITG 45A, indicating a field-star. The near-infrared spectrum of the primary contains Bγ absorption, also indicating a field-star.

Martín (2000) claims that the companion, ITG 45B, is also a field-star. However, the optical spectrum, as well as our near-infrared spectrum, is too noisy to classify it as a field-star or a YSO.

ITG 46

The location of ITG 46 in the HR diagram is unusual. Again, a large amount of veiling may lead to a high effective temperature. Otherwise, this object may be a field-star.

References

Aaronson, M., Frogel, J. A., & Persson, S. E. 1978, ApJ, 220, 442
Ali, B., Carr, J. S., DePoy, D. L., Frogel, J. A., & Sellgren, K. 1995, AJ, 110, 2415
Aspin, C., Sandell, G., & Russell, A. P. G. 1994, A&AS, 106, 165
Baraffe, I., Chabrier, G., Allard, F., & Hauschildt, P. H. 1998, A&A, 337, 403
Barsony, M., Kenyon, S. J., Lada, E. A., & Teuben, P. J. 1997, ApJS, 112, 109
Bertout, C., Basri, G., & Bouvier, J. 1988, ApJ, 330, 350
Bessell, M. S. 1991, AJ, 101, 662
Bessell, M. S., & Brett, J. M. 1988, PASP, 100, 1134
Briceño, C., Hartmann, L., Stauffer, J., & Martín, E. L. 1998, AJ, 115, 2074
Comeron, F., Rieke, G. H., Burrows, A., & Rieke, M. J. 1993, ApJ, 416, 185
Cushing, M. C., Tokunaga, A. T., & Kobayashi, N. 2000, AJ, 119, 3019
D'Antona, F., & Mazzitelli, I. 1994, ApJS, 90, 467
D'Antona, F., & Mazzitelli, I. 1997, Mem. Soc. Astron. Italiana, 68, 807
Dyck, H. M., van Belle, G. T., & Thompson, R. R. 1998 AJ, 116, 981
Elias, J. H. 1978, ApJ, 224, 857
Fluks, M. A., Plez, B., Thé, P. S., de Winter, D., Westerlund, B. E., & Steenman, H. C. 1994, A&AS, 105, 311
Gomez, M., Kenyon, S. J., & Hartmann, L. 1994, AJ, 107, 1850
Greene, T. P., & Lada, C. J. 1997, AJ, 114, 2157
Greene, T. P., & Meyer, M. R. 1995, ApJ, 450, 233
Gullbring, E., Petrov, P. P., Ilyin, I., Tuominen, I., Gahm, G. F., & Lodén, K. 1996, A&A, 314, 835
Itoh, Y., Tamura, M., & Gatley, I. 1996, ApJ, 465, L129 (ITG)
Itoh, Y., Tamura, M., & Nakajima, T. 1999, AJ, 117, 1471
Jones, H. R. A., Longmore, A. J., Jameson, R. F., & Mountain, C. M. 1994, MNRAS, 267, 413
Jones, T. J., Ashley, M., Hyland, A. R., & Ruelas-Mayorga, A. 1981, MNRAS, 197, 413
Kaifu, N., Usuda, T. Hayashi, S. S., Itoh, Y. Akiyama, M., Yamashita, T., Nakajima, Y., Tamura, M., et al. 2000, PASJ, 52, 1
Kenyon, S. J., & Hartmann, L. 1995, ApJS, 101, 117
Kim, C. Y. 1990, Memories of the Faculty of Kyoto University, Vol. 38, Series of Physics, Astrophysics and Chemistry, 1, 1
Kleinmann, S. G., & Hall, D. N. B. 1986, ApJS, 62, 501
Kobayashi, N., Tokunaga, A. T., Terada, H., Goto, M., Weber, M., Potter, R., Onaka, P. M., Ching, G. K., et al. 2000, Proc. SPIE, 4008, 1056
Koornneef, J. 1983, A&A, 128, 84
Koresko, C. D. 1998, ApJ, 507, L145
Lançon, A., & Rocca-Volmerange, B. 1992, A&AS, 96, 593
Leggett, S. K., Allard, F., Berriman, G., Dahn, C. C., & Hauschildt, P. H. 1996, ApJS, 104, 117
Lucas, P. W., & Roche, P. F. 2000, MNRAS, 314, 858
Lucas, P. W., Roche, P. F., Allard, F., & Hauschildt, P. H. 2001, MNRAS, 326, 695
Luhman, K. L. 2000, ApJ, 544, 1044
Luhman, K. L., Liebert, J., & Rieke, G. H. 1997, ApJ, 489, L165
Luhman, K. L., & Rieke, G. H. 1998, ApJ, 497, 354
Luhman, K. L., Rieke, G. H., Lada, C. J., & Lada, E. A. 1998, ApJ, 508, 347
Martín, E. L. 2000, AJ, 120, 2114
Martín, E. L., Dougados, C., Magnier, E., Ménard, F., Magazzù, A., Cuillandre, J.-C., Delfosse, X. 2001, ApJ, 561, L195
Meyer, M. R. 1996, PhD Thesis, University of Massachusetts
Meyer, M. R., Calvet, N., & Hillenbrand, L. A. 1997, AJ, 114, 288
Mountain, C. M., Robertson, D. J., Lee, T. J., & Wade, R. 1990, Proc. SPIE, 1235, 25
Najita, J., Carr, J. S., & Tokunaga, A. T. 1996, ApJ, 456, 292
Oasa, Y. 2001, PhD Thesis, The University of Tokyo
Oasa, Y., Tamura, M., & Sugitani, K. 1999, ApJ, 526, 336
Perrin, G., Coudé du Foresto, V., Ridgway, S. T., Mariotti, J.-M., Traub, W. A., Carleton, N. P., & Lacasse, M. G. 1998, A&A, 331, 619
Ramírez, S. V., DePoy, D. C., Frogel, J. A., Sellgren, K., & Blum, R. D. 1997, AJ, 113, 1411
Stapelfeldt, K., Krist, J. E., Ménard, F., Bouvier, J., Padgett, D. L., & Burrows, C. J. 1998, ApJ, 502, L65
Strom, K. M,, Kepner, J., & Strom, S. E. 1995, ApJ, 438, 813
Strom, K. M., Strom, S. E., Edwards, S., Cabrit, S., & Strutskie, M. F. 1989, AJ, 97, 1451
Strom, K. M., Strom, S. E., & Merrill, K. M. 1993, ApJ, 412, 233
Terndrup, D. M., Frogel, J. A., & Whitford, A. E. 1991, ApJ, 378, 742
Tokunaga, A. T. 2000, in Allen's Astrophysical Quantities, ed. A. N. Cox (NewYork: Springer-Verlag), 143
Tokunaga, A. T., Kobayashi, N., Bell, J., Ching, G. K., Hodapp, K.-W., Hora, J. L., Neill, D., Onaka, P. M., et al. 1998, Proc. SPIE, 3354, 512
Wichmann, R., Bastian, U., Krautter, J., Jankovics, I., & Rucinski, S. M. 1998, MNRAS, 301, L39
Wilking, B. A., Greene, T. P., & Meyer, M. R. 1999, AJ, 117, 469